

PAPER

Fully desktop fabricated flexible graphene electrocorticography (ECoG) arrays

To cite this article: Jia Hu *et al* 2023 *J. Neural Eng.* **20** 016019

View the [article online](#) for updates and enhancements.

You may also like

- [A system identification analysis of optogenetically evoked electrocorticography and cerebral blood flow responses](#)
Rex Chin-Hao Chen, Farid Atry, Thomas Richner et al.
- [Wireless opto-electro neural interface for experiments with small freely behaving animals](#)
Yaoyao Jia, Wasif Khan, Byunghun Lee et al.
- [Remapping cortical modulation for electrocorticographic brain-computer interfaces: a somatotopy-based approach in individuals with upper-limb paralysis](#)
Alan D Degenhart, Shivayogi V Hiremath, Ying Yang et al.



PAPER

Fully desktop fabricated flexible graphene electrocorticography (ECoG) arrays

RECEIVED
19 July 2022REVISED
13 December 2022ACCEPTED FOR PUBLICATION
22 December 2022PUBLISHED
18 January 2023Jia Hu^{1,6}, Ridwan Fayaz Hossain^{1,6}, Zahra S Navabi¹, Alana Tillery², Michael Laroque¹,
Preston D Donaldson³, Sarah L Swisher³ and Suhasa B Kodandaramaiah^{1,4,5,*} ¹ Department of Mechanical Engineering, University of Minnesota Twin Cities, Minneapolis, MN, 55455, United States of America² School of Medicine, Johns Hopkins University, Baltimore, MD, United States of America³ Department of Electrical and Computer Engineering, University of Minnesota Twin Cities, Minneapolis, MN, 55455, United States of America⁴ Department of Biomedical Engineering, University of Minnesota Twin Cities, Minneapolis, MN, 55455, United States of America⁵ Department of Neuroscience, University of Minnesota Twin Cities, Minneapolis, MN, 55455, United States of America⁶ Equal Contribution

* Author to whom any correspondence should be addressed.

E-mail: suhasabk@umn.edu

Keywords: Flexible, Graphene, ECoG

Supplementary material for this article is available [online](#)**Abstract**

Objective: Flexible ECoG electrode arrays that conform to the cortical surface and record surface field potentials from multiple brain regions provide unique insights into how computations occurring in distributed brain regions mediate behavior. Specialized microfabrication methods are required to produce flexible ECoG devices with high-density electrode arrays. However, these fabrication methods are challenging for scientists without access to cleanroom fabrication equipment. **Results:** Here we present a fully desktop fabricated flexible graphene ECoG array. First, we synthesized a stable, conductive ink via liquid exfoliation of Graphene in Cyrene. Next, we established a stencil-printing process for patterning the graphene ink via laser-cut stencils on flexible polyimide substrates. Benchtop tests indicate that the graphene electrodes have good conductivity of $\sim 1.1 \times 10^3 \text{ S cm}^{-1}$, flexibility to maintain their electrical connection under static bending, and electrochemical stability in a 15 d accelerated corrosion test. Chronically implanted graphene ECoG devices remain fully functional for up to 180 d, with average *in vivo* impedances of $24.72 \pm 95.23 \text{ k}\Omega$ at 1 kHz. The ECoG device can measure spontaneous surface field potentials from mice under awake and anesthetized states and sensory stimulus-evoked responses. **Significance:** The stencil-printing fabrication process can be used to create Graphene ECoG devices with customized electrode layouts within 24 h using commonly available laboratory equipment.

1. Introduction

Simultaneous neural computations occurring in many brain regions, and the interactions between these regions, mediate behavior [1–3]. Disruptions to these interactions are an indicator of neurological disorders such as Parkinson's disease [4] and traumatic brain injury [5]. Minimally invasive electrocorticography (ECoG) electrode arrays have been used to measure surface field potential generated by neural activity from several distributed populations of neurons in the cortex [6]. Functionally, ECoG electrode arrays covering large brain regions need to be flexible to make adequate contact with

the complex, convex surface of the brain [6, 7]. To this end, flexible, silicon substrate-based [8] and polymer substrate-based ECoG devices [7–19] have been developed. However, these devices were made using highly specialized micro- or nanofabrication techniques which require training and specialized fabrication equipment. Further, most neuroscience laboratories require rapid and flexible design alterations to adapt to various experimental contexts, which is hard to achieve with traditional microfabrication procedures. To simplify the fabrication procedure, inkjet printing conductive materials such as silver nanoparticle inks [9] and conductive polymer poly(3,4-ethylenedioxythiophene) polystyrene

sulfonate (PEDOT:PSS) ink [10] have been used to create flexible and reconfigurable ECoG electrode arrays. Currently, these approaches require expensive printers and still rely on specialized or microfabrication techniques to insulate the electrode [11].

This work introduces a fully-desktop fabricated, stencil-printed, flexible graphene ECoG electrode array, which is fabricated using commonly available equipment in neuroscience laboratories. Graphene has become an attractive material for fabricating neural interfaces [12–16] due to its high conductivity [17], flexibility [18], transparency [19], stability [20], and biocompatibility [18]. We first formulated a stable conductive ink based on exfoliating Graphene in Cyrene. The ink was then stencil-printed on a flexible polyimide (PI) substrate via laser-cut stencils. A similar procedure was applied to pattern a sacrificial layer of Pluronic, a triblock copolymer, for defining the exposed electrode pads. Lastly, a silicone elastomer insulation layer was coated on the electrodes using a custom-built, microprocessor-controlled spin-coater to create the functional ECoG electrode arrays. Most importantly, no aspect of the device fabrication needed access to specialized clean-room facilities. The flexible Graphene ECoG devices exhibited excellent benchtop performance characteristics and *in vivo* recording capabilities in chronically implanted mice with surface field potentials recorded for up to 180 d. Using this methodology, the proposed devices can be fabricated within 24 h and require a level of complexity and skill comparable to the assembly of tetrode devices [21].

2. Results

2.1. Desktop fabricated flexible graphene ECoG electrodes

We sought to engineer a flexible graphene ECoG device that could be entirely fabricated using commonly available equipment in neuroscience laboratories. Previous work has been done on stencil-printed graphene electronics [22–25], but fully desktop fabricated ECoG arrays implanted in mice have not been developed. First, the fabrication procedure required synthesizing a graphene ink to build the electrodes and retain electrical performance after chronic implantation. Secondly, we sought to establish a simple process for achieving reconfigurable electrode arrays for use in small animals. In this study, we used graphene exfoliated in Cyrene solvent to create a high-performance conductive ink that could be patterned on a PI film using a stencil-printing technique (figure 1(a)).

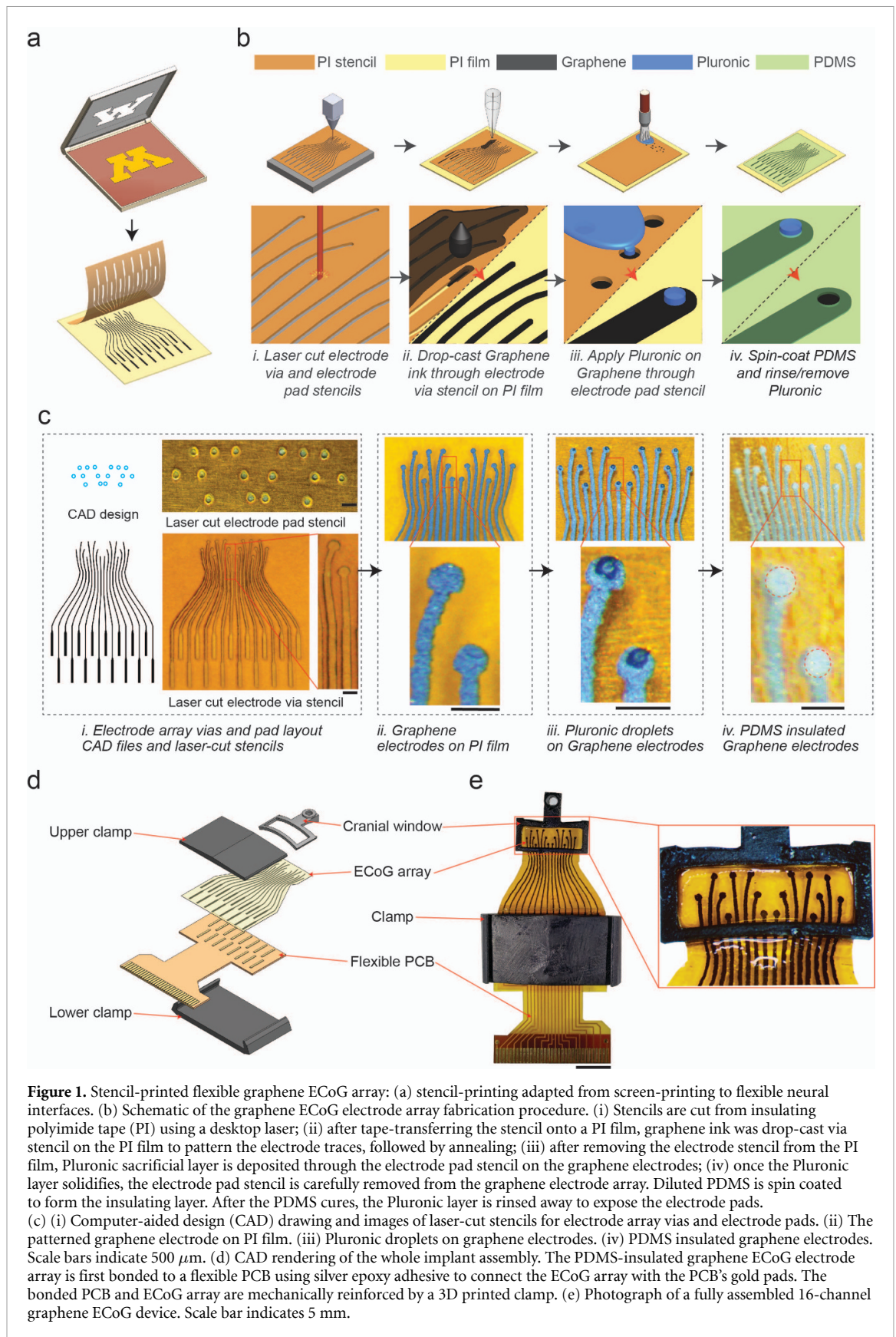
The overall fabrication procedure is shown in figure 1(a). In the first step, two stencils were created using a desktop laser cutter; one stencil for patterning the graphene electrodes, and the second for patterning the Pluronic sacrificial layer that defined the electrode pads (figure 1(a.i)). The desktop laser cutter

achieved a minimum inter-electrode (center to center) distance of $\sim 400 \mu\text{m}$. To reliably create isolated electrodes without any spurious interconnects, we used the minimum inter-electrode distance (center to center) of $\sim 500 \mu\text{m}$ in the stable design with electrode trace width of $\sim 200 \mu\text{m}$ (figures 1(b) and (c)). This inter-electrode distance ($500 \mu\text{m}$) depended on the laser power and cutting speed of the laser cutter, which was experimentally optimized (supplementary figure 1).

The first laser-cut stencil was overlaid on a flexible PI film, followed by drop-casting graphene ink to pattern the electrode arrays (figure 1(a.ii)). After drop-casting, the PI film with the stencil was annealed at a low temperature of $\sim 100 \text{ }^\circ\text{C}$ to evaporate the excess Cyrene solvent. Then, the stencil was stripped, and the electrode array was annealed at a high temperature of $\sim 300 \text{ }^\circ\text{C}$ (figure 1(c)). Once cooled to room temperature, the second stencil, for patterning the Pluronic sacrificial layer was overlaid on the substrate (figure 1(a.iii)). A fine paintbrush was used to apply Pluronic on the electrode pads through the second stencil (figure 1(a.iii)). After removing the stencil, the Pluronic layer was allowed to solidify overnight (figure 1(c.iii)). The graphene electrode array was then spin-coated with diluted silicone elastomer Polydimethylsiloxane (PDMS) to create the insulating layer. Once the elastomer was cured, the electrode array was gently rinsed in warm water to remove the Pluronic sacrificial layer covering the electrode pads, resulting in an PDMS-insulated electrode array with exposed electrode pads with an average diameter of $\sim 300 \mu\text{m}$ for interfacing the brain. The ECoG array also contains 16 electrode sites for interfacing with a printed circuit board (PCB) (supplementary figure 1(a)). Once the electrode arrays were fabricated, they were integrated into a 3D printed window frame adapted from our previous work [9, 26, 27]. The PCB interface was bonded to the ECoG array using conductive epoxy (supplementary figure 2(a)) and mechanically reinforced using a custom 3D printed clamp (figures 1(d) and (e)). The fabrication procedure relied entirely on common equipment such as a laser cutter and stereolithographic 3D printers, ubiquitous in nearly every university maker space. The electrode annealing was performed using a laboratory hotplate. Spin-coating was performed using a homebuilt microprocessor-controlled spinner (supplementary figure 5), but off-the-shelf low-cost speed-controllable spin coaters under \$1000 can also serve the purpose.

2.2. Formulation of graphene inks and material characterization

We formulated three graphene inks for stencil fabrication by exfoliating graphene in Cyrene, Dimethylformamide (DMF) [28–31], and Cyclohexanone/Terpineol (C/T) [18, 32, 33] solvents, using a top-down



liquid-phase exfoliation technique through ultrasonication (see section 4 for details). Graphene inks in DMF and C/T have already been used in optoelectronic, photovoltaic, and biomedical applications

[18, 29–34]. More recently, Cyrene demonstrated near-ideal physical properties for graphite exfoliation and the production of graphene dispersions [35]. For a sonication time of 2 h, Graphene exfoliated

in Cyrene resulted in drop-cast films with sub-micrometer surface flakes, whereas graphene exfoliated in DMF and C/T ink produced rougher films with much larger surface clusters (figure 2(a)). As shown in supplementary figure 6, the Raman spectroscopy was performed on spin-cast films from the three ink samples. The I_d/I_g ratio for highly disordered graphitic films like those generated from annealed graphene flakes increases with crystallite (i.e. flake) size [36]. The I_d/I_g ratio for the Cyrene-exfoliated graphene sample is the lowest, indicating it has the least average distance between defects (<1 nm), and that this sample is composed of the smallest flakes of the three inks, which were all annealed into a mainly sp^2 amorphous carbon structure [37]. Flake size is a determinant of the overall packing density, with a smaller flake size enhancing the inter-platelet connectivity, resulting in higher conductivity [18]. Further, smaller flake sizes are desirable for uniform patterning through stencils or inkjet printing if needed [18, 22]. The thickness of the drop-cast graphene inks were measured with a surface profiler to be $5.84 \mu\text{m}$ for Cyrene + Gr, $12.93 \mu\text{m}$ for C/T + EC + Gr, and $8.08 \mu\text{m}$ for DMF + EC + Gr (supplementary figure 7).

We next assessed the current–voltage characteristics of the three graphene films at room temperature (figure 2(b)). At 0.5 V, the current was measured to be ~ 61 mA for Cyrene + Gr, ~ 1.1 mA for DMF + EC + Gr, and ~ 0.2 mA for C/T + EC + Gr. Following the calculation in the method session, this finding corresponds to the highest conductivity of the Cyrene ink sample ($\sim 1.1 \times 10^3 \text{ s cm}^{-1}$). These results indicated that Cyrene was an adequate solvent for formulating the exfoliated graphene ink. The small flake size and high conductivity of Cyrene + Gr indicate its suitability for inkjet printing of electrodes [38] and as such, further experiments in this work involved devices made using graphene exfoliated in Cyrene.

2.3 Benchtop characterization of stencil fabricated graphene ECoG electrode arrays

Cyclic voltammetry (CV) was used to evaluate the electrochemical stability of graphene electrodes [39]. The CV of the graphene electrode ($n = 1$) was measured at potentials with scan rates ranging from 50 mV s^{-1} to 1000 mV s^{-1} . According to the shape of the plotted curves, both double-layer capacitance and pseudo-capacitance exist in the electrode (figure 2(e)) [40]. The capacitance value was extracted from the current (at 400 mV) vs. scan rate from the CV curve where the linear fit slope approximates the capacitance and was calculated to be ~ 10 nF at 400 mV.

Electrochemical impedance spectroscopy (EIS) measured over a frequency range of 1 Hz–10 kHz (figure 2(c)) was performed on a graphene ECoG device with 15 functional electrodes (We used a sample of 15 electrodes from one device to ensure the fabrication condition remains the same). The phase

angle shows the typical capacitive behavior (near 80°) at 20 Hz but gradually becomes more resistive at higher frequencies (figure 2(d)). At high frequencies ranging from 1 kHz to 10 kHz, the relatively low impedance magnitudes are attributed to the stray capacitance and the Ohmic resistance of the electrolyte solution and interconnect [41]. The EIS of the stencil-printed graphene electrode presents similar impedance characteristics as a previously reported ECoG array of monocrystalline graphene layers [14].

To evaluate the durability of the PDMS insulator and stability of graphene electrodes, we used ECoG arrays with 16 exposed electrode pads as the controls and the ECoG arrays with 16 electrode pads fully encapsulated with PDMS as the test device in accelerated corrosion test (figure 2(f)). Accelerated corrosion tests are typically used to evaluate the durability of devices by maintaining the devices in a 1X PBS solution for extended durations at high temperatures (60°C). Such tests simulate a fivefold acceleration in device degradation as compared to devices kept at physiological temperatures [42]. Based on these metrics, we performed accelerated corrosion tests lasting 15 d to evaluate the impedances for a projected 75 d period. At the end of the 15 d accelerated corrosion tests, the electrodes had an average impedance of $6.49 \pm 4.16 \text{ k}\Omega$ ($n = 16$) while devices fully encapsulated with PDMS all had impedances $> 1 \text{ M}\Omega$. These results indicate that the potential lifetime of the electrodes is at least 75 d at body temperature of 37°C .

The planar ECoG electrode array is typically bent to conform to the mouse's convex dorsal cortex with an approximate radius of curvature of 12 mm [26]. Therefore, it is important to investigate the relationship between the electrode impedance and the bending radii of curvature. The impedances of 9 identical, 10 mm long, straight, graphene electrodes were measured at 1 kHz while the electrodes were placed on a flat surface and then again when bent at various radii of curvature using a custom measurement rig (supplementary figure 3). No significant difference in the electrode impedance magnitudes could be found between electrodes placed on a flat surface and those at different radii of curvature (14 mm–6 mm) (figure 3(g)). Thus, the graphene electrodes patterned on the flexible PI substrates can be bent to conform to the dorsal cortical surface of the mouse brain with minimal effect on the electrode impedance.

2.3. *In vivo* experiments

The graphene ECoG devices were implanted on 4 mice to evaluate *in vivo* recording capabilities. The overall array dimensions were $\sim 9 \text{ mm} \times 4 \text{ mm}$, covering most of the sensory cortex areas bilaterally (figure 4(b)). Representative microscope images of one such implanted mouse taken on days 22 and 182 after implantation are shown in figure 3(a). No visible neuroimmune response such as Dural thickening and tissue encapsulation in these devices could

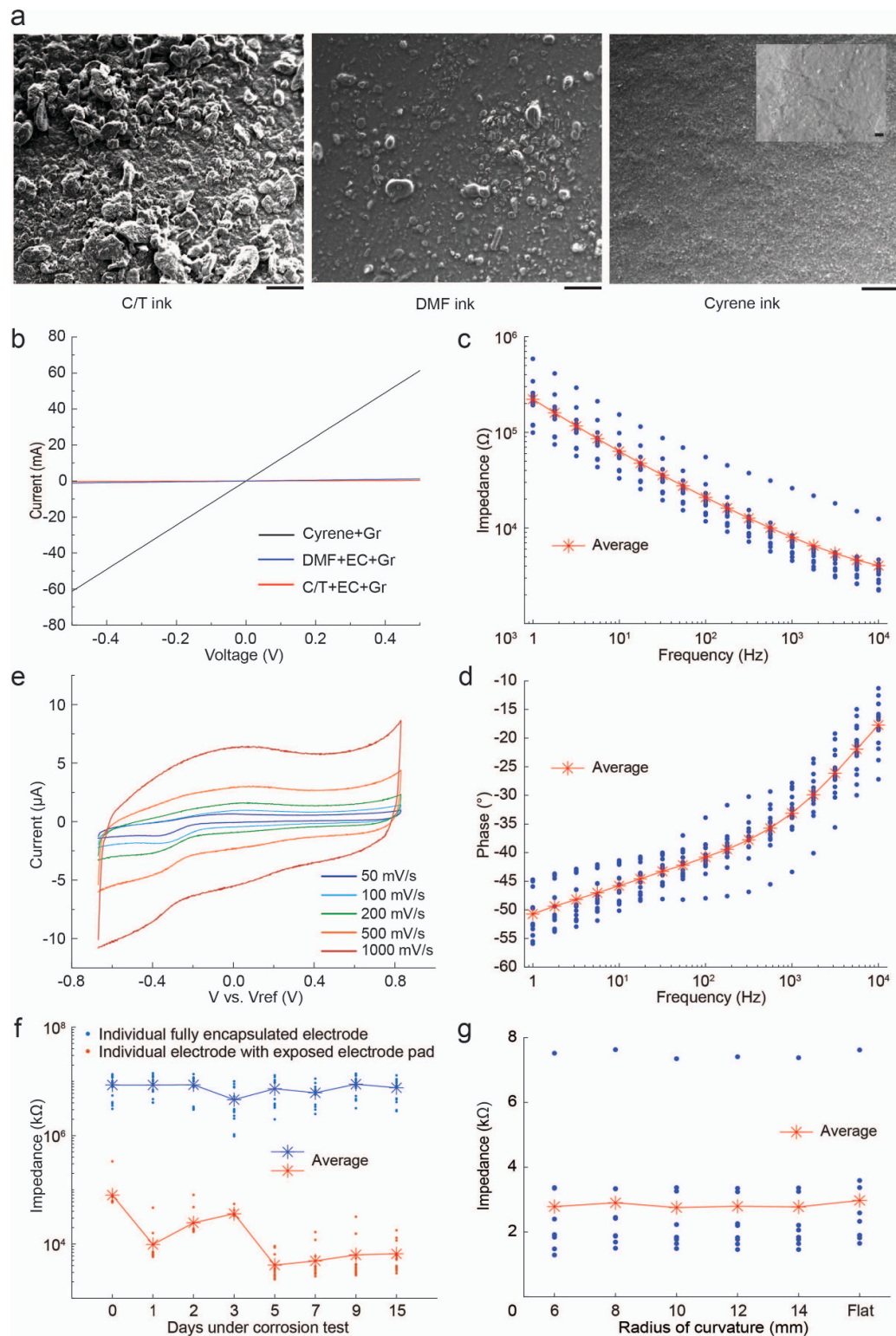
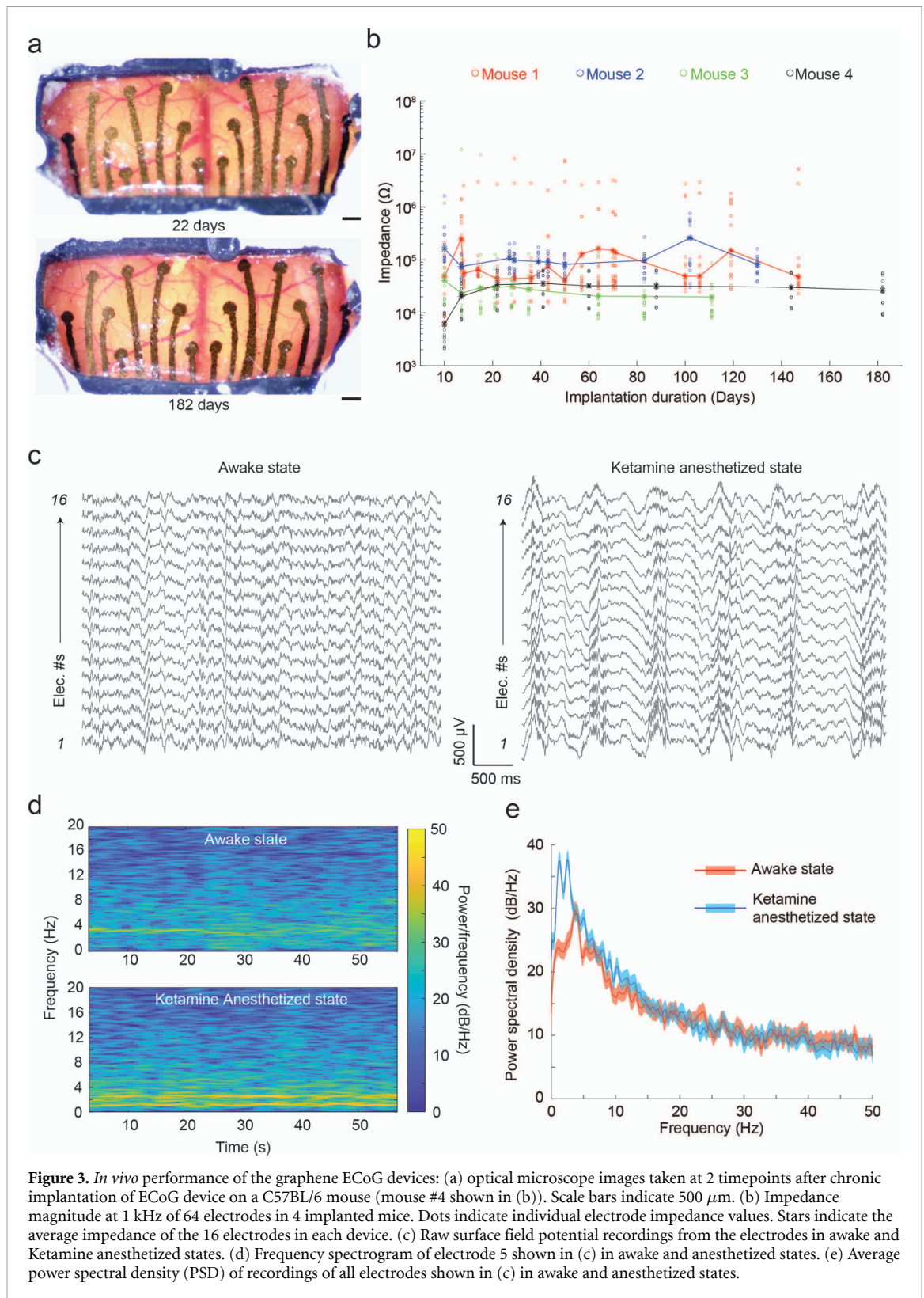
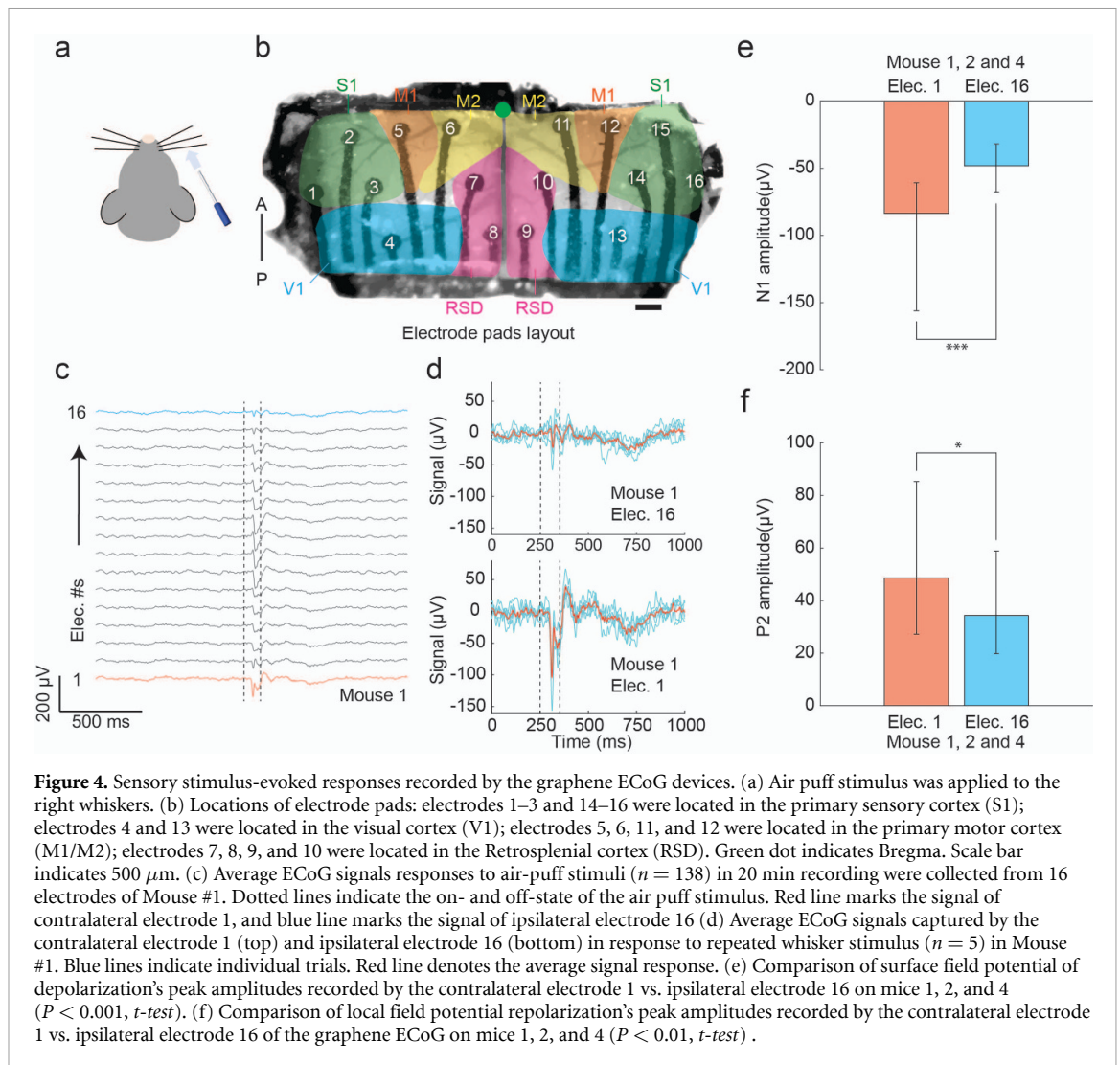


Figure 2. Material characterization of graphene films using three graphene inks and electrochemical characterization of graphene ECoG electrodes: (a) SEM images of the surface morphology of graphene films drop-cast onto a SiO₂/Si substrate. The inset in the top right image shows the higher magnification image. Scale bars indicate 200 μ m, while the scale bar in the inset indicates 2 μ m. (b) Current–voltage characteristics of three exfoliated graphene inks: graphene exfoliated in Cyrene (Cyrene + Gr), graphene exfoliated in Dimethylformamide with Ethyl Cellulose (DMF + EC + Gr), and graphene exfoliated in a mixture of Cyclohexanone and Terpineol with Ethyl Cellulose (C/T + EC + Gr). (c) Impedance magnitude, at frequencies ranging from 1 Hz to 10 kHz of ECoG electrodes made by stencil printing with Cyrene + graphene ink. (d) Phase angle at different frequencies ranging from 1 Hz to 10 kHz made by stencil printing with Cyrene + graphene ink. (e) Cyclic voltammetry of the graphene ECoG electrode in 1X PBS at different scan rates from 50 to 1000 mV s^{-1} . (f) Change in impedance magnitude as a function of time during an accelerated corrosion test. Each device has 16 electrodes with exposed electrode pads (red) and 16 electrodes with PDMS capsulated pads (blue). (g) The change of impedance magnitudes at 1 kHz as a function of radii of bending curvature for nine identical, 10 mm long, straight, graphene ECoG electrodes.



be found. Most of the inner surface of the implant was covered by a PDMS insulation layer (figure 1(c)). PDMS itself is a biocompatible material for long-term cranial implants [43]. The longest duration of implantation assessed was 21 weeks. The impedances of the electrodes were periodically measured throughout the implantation (figure 3(b)). Across 4 mice, 61 electrodes (out of 64) remained functional, with an

average impedance magnitude of $24.72 \pm 95.23 \text{ k}\Omega$ ($n = 61$) at 1 kHz. Three electrodes lost their connections on Mouse #1 at the measurement on day 10. Based on previous work describing a graphene ECoG device with similar electrode sizes, the impedance of functional ECoG electrodes was expected to be lower than 600 k Ω at 1 kHz [15]. The average electrode impedances of all four devices evaluated in this study



remained less than 600 k Ω throughout implantation ($n = 61/64$ electrodes). Therefore, our graphene electrode arrays can be used for chronic *in vivo* studies.

ECoG recordings were performed in head-fixed mice while fully awake and under Ketamine-anesthesia to demonstrate the functional use of the graphene ECoG devices. The raw recordings obtained from all 16 electrodes in both states are shown in figure 3(c). Consistent with previous observations [44–46], induction of the anesthetized state via Ketamine resulted in low-frequency oscillations at the delta frequency (0.5–4 Hz) throughout the cortex (figure 3(c)). These delta oscillations had signal peak-to-peak amplitudes of approximately 500 μV , much higher than the awake state's amplitude of ~ 200 μV (figure 3(c)). The spectrogram in figure 3(d) also presents a higher signal power density at 0.5–4 Hz at the anesthetized state, matching the power spectral density (PSD, figure 3(e)). The result indicates that all 16 channels of the device were functional to measure brain activity.

Furthermore, the graphene ECoG devices demonstrated the ECoG recordings of stimuli-evoked

brain activity in response to sensory stimuli. The stimuli were brief puffs of air (100 ms) given to the right whiskers of mice at randomized intervals during the awake state under head-fixation (figure 4(a)). Whisking and motor response were both observed in the experiments in response to the stimuli. Broad activation of most of the cortex in response to the stimuli was also observed and possibly caused by the startle response (figure 4(c)). Channels 1 and 16 were individually located at the contralateral and ipsilateral sensory cortices (S1) (figure 4(b)). Channel 1 showed higher signal amplitudes of negative peak N1 and positive peak P2 than channel 16 (figure 4(d)). Three animals (Mouse #1, Mouse #2, and Mouse #4) were used to analyze the signal difference between Channels 1 and 16. As shown in figures 4(e) and (f), the average N1 values in electrodes 1 vs. 16 were -83.60 ± 23.16 μV vs. -48.20 ± 12.29 μV ($p < 0.001$, t -test) on all three mice; the average P2 values in electrode 1 vs. 16 were 48.64 ± 19.96 μV vs. 34.34 ± 11.28 μV ($p < 0.05$, t -test) on all three mice. Both N1 and P2 values measured by electrode 1, placed on the left somatosensory cortex (contralateral

to the right whisker experienced air-puff stimulation), are significantly higher in amplitude than electrode 16, located on the right somatosensory cortex. Thus, the graphene ECoG electrode arrays successfully captured the evoked response to the lateral right whisker air-puff stimulation. These results are consistent with previous work done in our group [27].

3. Discussion

Here, we demonstrated for the first time a fully desktop-fabricated ECoG electrode array which we implanted on the rodent dorsal cortex for neurophysiological recording. The highly stable graphene ink formulated by exfoliating graphene in a biocompatible solvent Cyrene [47] demonstrated a high conductivity $\sim 1.1 \times 10^3 \text{ s cm}^{-1}$. Mechanical bending tests showed no significant change in electrode impedance at a flat surface and various radii of curvature ranging from 14 mm to 6 mm. Fully functional devices and the encapsulation of PDMS insulation were highly stable even under the accelerated aging environment, maintaining an average impedance of $\sim 6.49 \pm 4.16 \text{ k}\Omega$ on day 15. Furthermore, the electrodes remained functional with an average impedance magnitude of $24.72 \pm 95.23 \text{ k}\Omega$ (1 kHz) throughout the implantation. Thus, our graphene ECoG arrays provide robust neural interfaces that can be applied for chronic electrophysiology studies in mice.

To our knowledge, all the existing micrometer-scale ECoG devices are fully or partially fabricated using microfabrication or specialized techniques [42, 43, 48–55], resulting in high cost and low accessibility to neuroscience laboratories. In our method, the stencils determining the layout of the electrodes can be rapidly reconfigured using computer aided design (CAD) tools and fabricated using desktop laser-cutters available in most university fabrication shops. The graphene ink can be formulated using standard lab equipment, and the patterned electrodes can be sintered on a laboratory hotplate. The insulation layer can be deposited by a homebuilt, microcontroller-based spinner or a low-cost off-the-shelf spin coater. We have created the first fully desktop fabricated, flexible micrometer-scale ECoG array that can be chronically implanted in mice. These results point a way forward for creating robust, open-source, flexible neural interfaces that can be widely used in basic and translational neuroscience research.

Some limitations and concerns of the electrode characterization tests and results should be clarified and discussed. First, the conductivity of the Cyrene graphene electrode was measured to be $\sim 1.1 \times 10^5 \text{ s m}^{-1}$, which is sufficient for use in

neural probes, and is comparable to a PEDOT:PSS composite material ($3.23 \pm 0.75 \times 10^2 \text{ s m}^{-1}$) from a previous study [56]. However, the conductivity of the stencil-printed multilayer graphene electrode ($\sim 1.1 \times 10^5 \text{ s m}^{-1}$) is not comparable with monolayer graphene ($1.46 \pm 0.75 \times 10^6 \text{ s m}^{-1}$) synthesized by chemical vapor deposition [57]. To improve the conductivity of the ECoG electrode made by our desktop fabrication method, new conductive inks, such as inkjet printable gold nanoparticle ink ($8.0 \times 10^6 \text{ s m}^{-1}$), can be considered [58]. Secondly, for conducting the accelerated corrosion test, we used a 50 ml centrifuge tube that could only fit two devices with a total of 32 electrodes (one functional device consisting of partially PDMS-encapsulated graphene electrodes to evaluate the stability of the graphene electrodes and one device consisting of fully PDMS-encapsulated graphene electrodes to evaluate the durability of the PDMS insulation layer). Future studies with improved Graphene ECoG arrays can be evaluated with larger samples sizes. Further, the decrease in impedance values of graphene electrodes from day 0 to day 5 (figure 2(f)) might indicate vapor penetration through the PDMS insulation, which is water-repellent but permeable to water vapor [59]. To resolve this possible vapor penetration, alternate flexible insulation material, such as SU-8 [51], can be used instead. Thirdly, the impedance values ($24.72 \pm 95.23 \text{ k}\Omega$ at 1 kHz, $n = 61$) of the implanted ECoG devices have a high variability. One possible cause of this variability is the stencil printing fabrication method, where drop-casting the conductive ink through the laser-cut stencil made the thickness of the graphene electrodes difficult to control. To mitigate this, spin-coated or drop-casted PEDOT:PSS with smaller particle size can be explored in the future to reduce the impedance variability, as demonstrated previously [60].

We also identified some limitations to the proposed approach. First, the minimum feature size is limited by the resolution of the desktop laser cutter to create the stencils. Our ECoG devices with an inter-electrode (center to center) distance of $\sim 500 \mu\text{m}$ could be reliably patterned using the laser cutter, which limits the overall number and density of electrodes incorporated within a device. Second, the graphene ink needs to be annealed at high temperatures ($>300 \text{ }^\circ\text{C}$), limiting the type of substrate materials that can be used for supporting the graphene electrodes. As an alternative, photonic sintering can be used instead of thermal annealing, which would allow the use of substrate materials with low melting point, including transparent polymers such as polyethylene terephthalate. Patterning electrodes on transparent polymers creates devices for simultaneous imaging and ECoG recording [11] which currently require specialized equipment to

fabricate [48]. Our desktop-fabricated, stencil printing method has not yet been demonstrated on transparent graphene ECoG, but off-shelf transparent conductive PEDOT:PSS ink [8] can be a potential alternative for making fully transparent ECoG.

We would also like to note that while the fabrication procedure described here is well established in our group, direct implementation of the same may take some degree of optimization in the end-user labs. In our hands, synthesis of the ink takes 27 h, including a 24 h waiting period, and the ink can be stored and used for at least 2 months. One-time fabrication of 24 laser-cut masks takes 15 min, followed by 12 h, including an 8 h waiting period, for fabrication and assembly of 2–3 devices. It is especially critical to carefully perform the Pluronic deposition step of the fabrication procedure, which can result in failure due to misalignment of the Pluronic sacrificial layer and the graphene electrode pads. These are necessary considerations for achieving high-performance devices. It must be noted that laser-induced graphene [61] may be more efficient to pattern electrodes but the laser-induced graphene itself still requires specialized microfabrication methods which may not be accessible to all end user laboratories.

Several directions can be pursued in the future, building upon the graphene ECoG devices presented in this work. The size of the implant can be extended to much larger regions of the brain [26, 27] so that the whole visual cortex and motor cortex can be included for performing ECoG recording over most of the cortical surface of the mouse brain [11]. The low and stable impedance of the electrodes can be leveraged for precise cortical micro-stimulation [14]. Miniaturization of electronic interface circuits can also allow deployment in freely behaving animals, potentially combined with imaging instrumentation for simultaneously tracking large-scale calcium dynamics [27]. Further, graphene has shown utility in passive sensing of electrical potentials and functionalizing to highly sensitive biochemical sensing [62]. Overall, our method can be scaled to mass manufacturing of flexible graphene-based biosensors at a low cost with a myriad of applications in biological sensing, such as electrocardiography [63], electromyography [64], and peripheral nerve interfacing [65].

4. Methods

4.1. Graphene inks formulation

The graphene inks were formulated by bath ultra-sonication of graphene powder, which was ground using a mortar and pestle from a graphite rod (496 561, Sigma Aldrich), in a mixture of C/T (398 241 and 814 759, Sigma Aldrich) at a ratio of 7:3, DMF(319 937, Sigma Aldrich), and Cyrene (807 796, Sigma Aldrich). An initial concentration of Ethyl Cellulose (EC) (EC 200 646, Sigma Aldrich) at 2.5 wt% and 10 mg mL⁻¹ graphene powder were then

added in 10 ml C/T and DMF, treated for 2 h in the Branson Bath Sonicator (CPX2800, Fisher Scientific) at 30 °C. No EC was added to the Cyrene ink as it produces excess bubbles resulting in bad drop casting. All three dispersions were kept idle for 24 h to precipitate the larger particles, which left pale gray precipitation at the bottom of the vials. The supernatant (~ 8 ml) inks were extracted and stored in clean vials.

4.2. Graphene sample preparation for Electrical Measurement

To carry out the initial electrical characterization of the graphene inks, high integrity metal contacts composed of silver (Ag) were first patterned with photolithography and deposited with an e-beam evaporator on the PI film, followed by drop-casting of 0.5 ml graphene ink in a rectangular area of 10.5 mm × 2 mm using a stencil (supplementary figure 4). The sample was annealed at 350 °C for 90 min. A probe station with parameter analyzer (B1500A, Agilent Technologies) was used to conduct 2-point-probe voltage-controlled measurements and data extraction to evaluate the current–voltage characteristics of three graphene films (figure 2(b)). The current density (A cm⁻²) was calculated from the measured current values (A) (figure 2(b)) divided by the cross-section area of the sample of 1.17 × 10⁻⁴ cm² (sample width of 2 mm × sample thickness of 5.84 μm of Cyrene graphene). The electric field (V cm⁻¹) was defined as applied voltage (V) (figure 2(b)) divided by the sample length of 1.05 cm. The conductivity (S cm⁻¹) of the graphene sample was calculated by dividing the current density (A cm⁻²) by the electric field (V cm⁻¹).

4.3. Electrode array design and assembly

4.3.1. Electrode array design

The layout of the graphene electrode array was rendered in computer-aided design software (SolidWorks 2021, Dassault) (figure 1(c)). The center-to-center distances between two neighboring electrode pads ranged from ~600 μm to 1 mm. The overall layout of the electrode array was designed to cover an area of ~9 mm long, extending bilaterally, with a width of ~4 mm posterior to Bregma (figure 4(b)). Electrodes 1–3 and 14–16 were in the primary sensory cortex (S1); electrodes 4 and 13 were located in the visual cortex (V1); electrodes 5–6 and 11–12 were located in the primary motor cortex (M1/M2), and 7–10 were located in Retrosplenial cortex.

4.3.2. Laser-cut stencils

To fabricate the stencils, a piece of 50 μm-thick insulating PI tape (High Temperature Tape, Bertech) with a size of 25.4 mm by 160 mm was adhered to a stainless-steel sheet and subsequently patterned by a CO₂ laser cutter (PLS6.140D, Universal System)

(figure 1(a)). We tested the laser cutter's cutting precision on the PI tape and found that the inter-electrode pitch (center to center distance) of $\sim 500 \mu\text{m}$ with power settings of 10% and speed settings of 100% can consistently fabricate the stencils used in this study (supplementary figure 1(b)). The electrode via stencil was transferred to a PI film substrate using a scotch tape transfer method modified from previous work [66].

4.3.3. Graphene ink deposition

The graphene ink was manually drop-cast on the laser-cut mask and annealed at a high temperature ($\sim 350^\circ\text{C}$) for 90 min. To evaporate the solvent completely, the hotplate temperature was ramped at $\sim 10^\circ\text{C min}^{-1}$ from 100°C to 330°C to evaporate the solvent completely. After annealing, the mask was carefully removed, leaving the patterned graphene channels on the PI film. A similar procedure was used to apply a sacrificial layer of Pluronic, a triblock copolymer, (F-127, Sigma Aldrich) after manually aligning the electrode pad stencil to the graphene electrodes. The sample was kept overnight at room temperature to solidify the Pluronic. Diluted PDMS was spin-coated at 1500 rpm for 15 s using a home-built desktop spin-coater (supplementary figure 5), then cured at 30°C temperature for 15 min. For making the diluted PDMS, the tert-Butanol (471 712, Sigma) was warmed at 45°C and mixed with PDMS and SYLGARD 184 curing agent (761 036, Sigma) at the weight ratio of 50:10:1. The Pluronic was rinsed away with a gentle flow of hot water at 45°C – 60°C to expose the electrode pads. Then the sample was annealed again at 100°C for 30 min.

4.3.4. Implant assembly

The graphene ECoG device is an assembly of four major components: the stencil fabricated ECoG array, a 3D printed cranial window frame, a flexible PCB connector, and a 3D printed reinforcement clamp. The cranial window frame and the reinforcement clamps were 3D-printed using a stereolithography 3D printer (Form 2, Formlabs). The PCB connector was custom-designed in Eagle (Autodesk Inc.) and fabricated by an online printed circuit board (PCB) manufacturer (PCBWay.com). To assemble the device, the ECoG electrode array was first bonded to the gold soldering pads on the flexible PCB connector using a conductive adhesive (8331 Silver Epoxy Adhesive, MG Chemical) (supplementary figure 2) by applying it manually with a sharp object. The interface was further mechanically reinforced using the 3D-printed clamp and followed by encapsulation with clear epoxy adhesive (Scotch-Weld Epoxy Adhesive DP100 Plus, 3 M). The recording area of the stencil fabricated graphene electrode arrays was bonded to a 3D printed cranial window frame using epoxy adhesive (DP1000

Plus Clear, 3 M) adapted from our previous work [26, 27] to realize the device illustrated in figure 1(e). The cranial window defined a total recording area of $\sim 4 \text{ mm} \times 9 \text{ mm}$, with a radius of curvature of 10 mm, to allow conformal implantation over the dorsal cortex immediately posterior to Bregma (figure 4(b)). A fully assembled device has a mass of $\sim 1.3 \text{ g}$.

4.4. Benchtop testing of fully assembled devices

CV (figure 2(b)), EIS (figures 2(c) and (d)), and accelerated corrosion tests (figure 2(f)) were performed on fully assembled graphene ECoG devices. EIS and CV measurements were conducted using a potentiostat (1010E, Gamry Instruments), with an Ag/AgCl reference electrode (Gamry Instruments) and a platinum wire as a counter electrode (1.0 mm diameter, Premion, 99.997%, Alfa Aesar) in room temperature 1X Phosphate Buffered Saline solution (D1408 PBS 10X, Sigma-Aldrich). EIS was performed with a 50 mV excitation voltage from 10 kHz to 1 Hz. Ten measurements were taken per decade. The CV was performed at varying scan rates from 50 to 1000 mV s^{-1} , with voltage limits set at $\pm 0.75 \text{ V}$ vs. the open circuit potential.

The accelerated corrosion test was performed [67] by immersing two ECoG devices (one device has 16 exposed electrode pads, and one device has 16 fully PDMS-capsulated electrode pads) into 1X Phosphate-buffered saline (D1408 PBS 10X, Sigma-Aldrich) at an elevated temperature of 60°C which is equivalent to a five-fold accelerated corrosion process at body temperature of 37°C [42]. Impedances of the device were measured using the interface board (RHD2000, Intan Technologies) at 1 kHz daily for 2 weeks.

Bending testing was conducted by creating 9 straight, parallel graphene electrodes using the same ECoG stencil printing technique. To mimic various degrees of bending after implantation, the electrodes were placed on a flat surface and custom-built acrylic structures (supplementary figure 3) with radii of curvature of 6 mm, 8 mm, 10 mm, 12 mm, and 14 mm, while their impedance was measured using the interface board (RHD2000, Intan Technologies Inc.) at 1 kHz.

4.5. Surgical implantation

All animal experiments were approved by the University of Minnesota Intuitional Animal Care and Use Committee (IACUC). 9 C57BL/6 mice (5 males and 4 females) at the age of 12–30 weeks were used in this study. Initially, 5 mice were implanted with the graphene ECoG devices during the optimization of the electrode layout and overall device design. Mice were housed in a 14 h light/10 h dark cycle in rooms maintained at 20°C – 23°C and 30%–70% relative humidity. Mice had ad libitum

access to food and water. Mice were given preemptive doses of 2 mg kg^{-1} of sustained-release buprenorphine (Buprenorphine SR-LAB, ZooPharm) and 2 mg kg^{-1} of meloxicam for analgesia and preventing brain inflammation, respectively. Mice were anesthetized 30–60 min after the initial analgesia dosage using 1%–5% isoflurane anesthesia in Oxygen. Eye ointment (Puralube, Dechra Veterinary Products) was applied to the eyes. The scalp was shaved and cleaned. Once the mice were fixed in a stereotax (900LS, Kopf), the scalp was sterilized by repeatedly scrubbing Betadine and 70% Ethanol solution (3 times). Next, the scalp was removed using surgical scissors. The tissue and fat under the scalp were subsequently cleared using a micro curette (#10080–05; Fine Science Tools). Partial temporalis muscle wrapping around the skull was carefully removed using a scalpel to expose the squamosal area. After drilling a $\sim 300 \mu\text{m}$ -diameter hole on the squamosal suture, a stainless-steel bone screw (#FF000CE094, JI MORRIS Company) tied to a 26-gauge stainless-steel reference wire was tightened in the hole firmly. A large craniotomy was immediately performed using a high-speed dental drill following a rectangular path approximately $4 \text{ mm} \times 9 \text{ mm}$ posterior to Bregma. After the drilling, the skull piece was removed from the dorsal cortex using two micro curettes holding its lateral edges. A gauze pad soaked in sterile saline was gently placed on the exposed brain to keep it moist.

The graphene ECoG device was sterilized by immersion in 70% Ethanol for 2 min and subsequently rinsed thoroughly with sterile saline. The periphery of the craniotomy was cleaned using a pointed cotton tip after removing the gauze pad. The window frame was gently placed on the exposed brain. Surgical adhesive (Vetbond, 3 M) was applied around the edges of the window frame to bond the window frame to the skull. After the adhesive was cured, a customized waterjet-cut Titanium headplate was fastened on the implant with a #0–80 screw. The implant was cemented to the skull using opaque dental cement (Metabond, Parkell Inc.). Mice were transferred from the stereotax to a heated pad (catalog no. 72–0492; Harvard Apparatus) for recovery from the anesthesia and were transferred to a clean cage partially located on a warming pad once they were fully ambulatory. 2 mg kg^{-1} meloxicam was administered twice per 24 h for 72 h post-surgery. Mice recovered for 7 d before any *in vivo* experiment.

4.6. *In vivo* electrophysiology

In vivo electrode performance test: The impedances of electrodes in the implanted devices were measured periodically (up to 182 d). Animals were transferred from their home cage and affixed under anesthesia in a custom head-fixation device adapted from previous studies [26, 68]. Subsequently, the flexible printed circuit (FPC) connector on the amplifier was connected

to the PCB connector of the ECoG device. Impedance measurements were acquired at 1 kHz.

4.3.1. *Awake and anesthetized spontaneous recordings*

Mice were head-fixed on the treadmill, and 4 min of spontaneous recordings were acquired when the animals were fully awake. All the signals were recorded through the interface board (RHD 200, Intan Technologies Inc.) at a sampling rate of 20 kHz. Mice were administered a cocktail of Ketamine (100 mg kg^{-1}) and xylazine (10 mg kg^{-1}) while head-fixed. A heated pad was placed under the animal to maintain body temperature, and mice were supplemented with Oxygen. Once the animal was fully unresponsive to toe pinch stimulus, multiple 4 minute-long spontaneous recordings were acquired. Once fully recovered from anesthesia, mice were removed from the head fixation apparatus and transferred back to their home cage.

4.3.2. *ECoG recordings in response to sensory stimuli*

Stimulation applied to mice whiskers is a common way to study the evoked response in the somatosensory system [69]. Here, we used a lateral air-puff stimulation to test whether the implanted ECoG array can successfully measure the contralateral evoked response [27]. To do so, brief air-puff stimuli of compressed air flow were applied to the right whiskers of head-fix mice through a blunt 24-gauge stainless steel needle. The needle guided the air-puff to stimulate the whiskers in the posterior-anterior direction (figure 4(a)). In each experimental session, each mouse received 24–30 air-puff stimuli with 100 ms duration. The inter-stimulus interval was randomized (8–10 s) and controlled using a micro-controller (Arduino Uno, Adafruit) actuated solenoid valve.

4.7. Data analysis

All the data, including electrode impedances and ECoG signals, were collected and converted using the interface board's software (RHD2000 interface, Intan Technologies Inc.). The raw ECoG signals were first down-sampled to a moving average of 2 kHz and low-pass filtered using an elliptic filter with a passband of 100 Hz. Custom scripts in MATLAB (MATLAB 2020b, MathWorks) were used to analyze and plot the data.

Author contributions

S B K conceived the overall project. J H, R F H, A T, and S B K conceptualized the devices. J H developed the electrode array designs, laser-cut stencil technique, implant, and electrode interface. J H also designed and performed the *in vivo* experiments, surgical implantation, and data analysis with the help of Z N R F H developed the recipe for the graphene inks and characterized the properties. R F H performed

the electrical & material characterization and analysis. R F H also engineered and developed the stencil fabrication process of the ECoG electrode array and cleanroom fabrication of the test samples. J H and R F H performed the electrode bending test. P D D carried out CV and EIS experiments with the help of R F H and J H, M L designed and built the spin coater. J H, R F H, P D D and S B K wrote the paper. All authors revised and contributed to the final manuscript.

Data availability statement

The data that support the findings of this study are available upon reasonable request from the authors.

Acknowledgments

SBK and SLS acknowledge NINDS Award #R01NS111028. SBK acknowledges Brain Initiative Award R42NS110165. Parts of this work were carried out in the Characterization Facility, at the University of Minnesota, which receives partial support from the NSF through the MRSEC (Award Number DMR-2011401) and the NNCI (Award Number ECCS-2025124) programs. Portions of this work were conducted in the Minnesota Nano Center, which is supported by the National Science Foundation through the National Nanotechnology Coordinated Infrastructure (NNCI) under Award Number ECCS-2025124. We acknowledge Javier Garcia Barriocanal for assistance with the XRD measurements. PDD was supported by NSF IGERT Award DGE-1069104. Skylar Fausner for assistance with animal preparation. We thank Skylar Fausner, Beatrice Gulner, and James Hope for useful comments and critiques of the paper.

Institutional Approval

All animal experiments described in this paper were approved by the University of Minnesota's Institutional Animal Care and Use Committee (IACUC).

Conflict of interest

The authors declare no competing interests.

ORCID iD

Suhasa B Kodandaramaiah 
<https://orcid.org/0000-0002-7767-2644>

References

- [1] Torres I 1995 Human behavior and the developing brain *Am. J. Psychiatry* **152** 637–a
- [2] Moustafa A 2017 *Computational Models of Brain and Behavior* 1st edn (Hoboken, NJ: Wiley-Blackwell) (<https://doi.org/10.1002/9781119159193>)
- [3] West S L et al 2021 Wide-field calcium imaging of dynamic cortical networks during locomotion *Cereb. Cortex* **32** 2668–87
- [4] Bijsterbosch J D, Woolrich M W, Glasser M F, Robinson E C, Beckmann C F, Van Essen D C, Harrison S J and Smith S M 2018 The relationship between spatial configuration and functional connectivity of brain regions *Elife* **7** e32992
- [5] Cramer S W et al 2023 Wide-field calcium imaging reveals widespread changes in cortical connectivity following repetitive, mild traumatic brain injury in the mouse *Neurobiol. Dis.* **176** 105943
- [6] Kim J, Lee M, Rhim J S, Wang P, Lu N and Kim D H 2014 Next-generation flexible neural and cardiac electrode arrays *Biomed. Eng. Lett.* **4** 95–108
- [7] Khodagholy D, Gelinas J N, Thesen T, Doyle W, Devinsky O, Malliaras G G and Buzsáki G 2015 NeuroGrid: recording action potentials from the surface of the brain *Nat. Neurosci.* **18** 310–5
- [8] Rachinskiy I, Wong L, Chiang C-H, Wang C, Trumpis M, Ogren J I, Hu Z, McLaughlin B and Viventi J 2022 High-density, actively multiplexed μ ECoG array on reinforced silicone substrate *Front. Nanosci.* **4** 837328
- [9] Donaldson P D, Ghanbari L, Rynes M L, Kodandaramaiah S B and Swisher S L 2019 Inkjet-printed silver electrode array for *in-vivo* electrocorticography *Int. IEEE/EMBS Conf. on Neural Engineering, NER* vol 2019
- [10] Donaldson P D and Swisher S L 2022 Transparent, low-impedance inkjet-printed pedot:pss microelectrodes for multimodal neuroscience *Phys. Status Solidi a* **219** 2100683
- [11] Donaldson P D et al 2022 Polymer skulls with integrated transparent electrode arrays for cortex-wide opto-electrophysiological recordings *Adv. Healthcare Mater.* **11** 2200626
- [12] Ryu M et al 2017 Enhancement of interface characteristics of neural probe based on graphene, ZnO nanowires, and conducting polymer PEDOT *ACS Appl. Mater. Interfaces* **9** 10577–86
- [13] Bourrier A et al 2019 Monolayer graphene coating of intracortical probes for long-lasting neural activity monitoring *Adv. Healthcare Mater.* **8** 1801331
- [14] Park D W et al 2018 Electrical neural stimulation and simultaneous *in vivo* monitoring with transparent graphene electrode arrays implanted in GCaMP6f mice *ACS Nano* **12** 148–57
- [15] Park D W et al 2014 Graphene-based carbon-layered electrode array technology for neural imaging and optogenetic applications *Nat. Commun.* **5** 1–11
- [16] Kuzum D et al 2014 Transparent and flexible low noise graphene electrodes for simultaneous electrophysiology and neuroimaging *Nat. Commun.* **5** 1–10
- [17] Geim A K and Novoselov K S 2007 The rise of graphene *Nat. Mater.* **6** 183–91
- [18] Hossain R F, Deaguero I G, Boland T and Kaul A B 2017 Biocompatible, large-format, inkjet printed heterostructure MoS₂-graphene photodetectors on conformable substrates *npj 2D Mater. Appl.* **1** 1–10
- [19] Nair R R, Blake P, Grigorenko A N, Novoselov K S, Booth T J, Stauber T, Peres N M R and Geim A K 2008 Fine structure constant defines visual transparency of graphene *Science* **320** 1308
- [20] Cristarella T C, Chinderle A J, Hui J and Rodríguez-López J 2015 Single-layer graphene as a stable and transparent electrode for nonaqueous radical annihilation electrogenerated chemiluminescence *Langmuir* **31** 3999–4007
- [21] Voigts J, Siegle J, Pritchett D L and Moore C I 2013 The flexDrive: an ultra-light implant for optical control and highly parallel chronic recording of neuronal ensembles in freely moving mice *Front. Syst. Neurosci.* **7** 8
- [22] Hyun W J, Secor E B, Hersam M C, Frisbie C D and Francis L F 2015 High-resolution patterning of graphene by

- screen printing with a silicon stencil for highly flexible printed electronics *Adv. Mater.* **27** 109–15
- [23] Xu Y, Schwab M G, Strudwick A J, Hennig I, Feng X, Wu Z and Müllen K 2013 Screen-printable thin film supercapacitor device utilizing graphene/polyaniline inks *Adv. Energy Mater.* **3** 1035–40
- [24] Yong K, Ashraf A, Kang P and Nam S 2016 Rapid stencil mask fabrication enabled one-step polymer-free graphene patterning and direct transfer for flexible graphene devices *Sci. Rep.* **6** 1–8
- [25] Jabari E, Ahmed F, Liravi F, Secor E B, Lin L and Toyserkani E 2019 2D printing of graphene: a review *2D Mater.* **6** 042004
- [26] Ghanbari L et al 2019 Cortex-wide neural interfacing via transparent polymer skulls *Nat. Commun.* **10** 1–13
- [27] Rynes M L et al 2021 Miniaturized head-mounted microscope for whole-cortex mesoscale imaging in freely behaving mice *Nat. Methods* **18** 417–25
- [28] Htwe Y Z N, Abdullah M K and Mariatti M 2021 Optimization of graphene conductive ink using solvent exchange techniques for flexible electronics applications *Synth. Met.* **274** 116719
- [29] Alamri A M, Leung S, Vaseem M, Shamim A and He J-H 2019 Fully inkjet-printed photodetector using a graphene/perovskite/graphene heterostructure *IEEE Trans. Electron Devices* **66** 2657–61
- [30] Casaluci S, Gemmi M, Pellegrini V, Di Carlo A and Bonaccorso F 2016 Graphene-based large area dye-sensitized solar cell modules *Nanoscale* **8** 5368–78
- [31] Silva M, Pinho I S, Covas J A, Alves N M and Paiva M C 2021 3D printing of graphene-based polymeric nanocomposites for biomedical applications *Funct. Compos. Mater.* **2** 1–21
- [32] Fang Y, Hester J G D, Su W, Chow J H, Sitaraman S K and Tentzeris M M 2016 A bio-enabled maximally mild layer-by-layer kapton surface modification approach for the fabrication of all-inkjet-printed flexible electronic devices *Sci. Rep.* **6** 1–9
- [33] Secor E B, Prabhumirashi P L, Puntambekar K, Geier M L and Hersam M C 2013 Inkjet printing of high conductivity, flexible graphene patterns *J. Phys. Chem. Lett.* **4** 1347–51
- [34] Michel M, Biswas C and Kaul A B 2017 High-performance ink-jet printed graphene resistors formed with environmentally-friendly surfactant-free inks for extreme thermal environments *Appl. Mater. Today* **6** 16–21
- [35] Pan K, Fan Y, Leng T, Li J, Xin Z, Zhang J, Hao L, Gallop J, Novoselov K S and Hu Z 2018 Sustainable production of highly conductive multilayer graphene ink for wireless connectivity and IoT applications *Nat. Commun.* **9** 1–10
- [36] Lucchese M M, Stavale F, Ferreira E H M, Vilani C, Moutinho M V O, Capaz R B, Achete C A and Jorio A 2010 Quantifying ion-induced defects and Raman relaxation length in graphene *Carbon* **48** 1592–7
- [37] Childres I, Jauregui L A, Park W, Caoa H and Chena Y P 2013 Raman spectroscopy of graphene and related materials *New Developments in Photon and Materials Research*
- [38] Hossain R F and Kaul A B 2018 Biocompatible, inkjet printed heterostructure photodetector for biosensing applications 2018 31st Annual Conf. IEEE Photonics Society, IPC (<https://doi.org/10.1109/IPCCon.2018.8527301>)
- [39] Cogan S F 2008 Neural stimulation and recording electrodes *Annu. Rev. Biomed. Eng.* **10** 275–309
- [40] Shao Y, Wang H, Zhang Q and Li Y 2014 Fabrication of large-area and high-crystallinity photoreduced graphene oxide films via reconstructed two-dimensional multilayer structures *NPG Asia Mater.* **6** e119
- [41] Yagati A K, Min J and Cho S 2014 Electrosynthesis of ERGO-NP nanocomposite films for bioelectrocatalysis of horseradish peroxidase towards H₂O₂ *J. Electrochem. Soc.* **161** G133–40
- [42] Woods V, Trumpis M, Bent B, Palopoli-Trojani K, Chiang C-H, Wang C, Yu C, Insanally M N, Froemke R C and Viventi J 2018 Long-term recording reliability of liquid crystal polymer μ ECoG arrays *J. Neural. Eng.* **15** 066024
- [43] Lee W R, Im C, Koh C S, Kim J M, Shin H C and Seo J M 2017 A convex-shaped, PDMS-parylene hybrid multichannel ECoG-electrode array *Proc. Annual Int. Conf. IEEE Engineering in Medicine and Biology Society, EMBS* (<https://doi.org/10.1109/EMBC.2017.8037018>)
- [44] Michelson N J and Kozai T D Y 2018 Isoflurane and ketamine differentially influence spontaneous and evoked laminar electrophysiology in mouse V1 *J. Neurophysiol.* **120** 2232–45
- [45] Fontanini A, Spano P F and Bower J M 2003 Ketamine-xylazine-induced slow (<1.5Hz) oscillations in the rat piriform (olfactory) cortex are functionally correlated with respiration *J. Neurosci.* **23** 7993–8001
- [46] Hwang E, McNally J M and Choi J H 2013 Reduction in cortical gamma synchrony during depolarized state of slow wave activity in mice *Front. Syst. Neurosci.* **7** 107
- [47] Grune C, Thamm J, Werz O and Fischer D 2021 Cyrene™ as an alternative sustainable solvent for the preparation of poly(lactic-co-glycolic acid) nanoparticles *J. Pharm. Sci.* **110** 959–64
- [48] Ledochowitsch P, Olivero E, Blanche T and Maharbiz M M 2011 A transparent ECoG array for simultaneous recording and optogenetic stimulation *Proc. Annual Int. Conf. IEEE Engineering in Medicine and Biology Society, EMBS* (<https://doi.org/10.1109/IEMBS.2011.6090808>)
- [49] Kwon K Y, Sirowatka B, Weber A and Li W 2013 Opto- μ ECoG array: a hybrid neural interface with transparent μ ECoG electrode array and integrated LEDs for optogenetics *IEEE Trans. Biomed. Circuits Syst.* **7** 593–600
- [50] Yang W, Gong Y, Yao C-Y, Shrestha M, Jia Y, Qiu Z, Fan Q H, Weber A and Li W 2021 A fully transparent, flexible PEDOT:PSS-ITO-Ag-ITO based microelectrode array for ECoG recording *Lab Chip* **21** 1096–108
- [51] Márton G, Orbán G, Kiss M, Fiáth R, Pongrácz A and Ulbert I 2015 A multimodal, SU-8—Platinum—Polyimide microelectrode array for chronic *in vivo* neurophysiology *PLoS One* **10** e0145307
- [52] Yeager J D, Phillips D J, Rector D M and Bahr D F 2008 Characterization of flexible ECoG electrode arrays for chronic recording in awake rats *J. Neurosci. Methods* **173** 279–85
- [53] Vomero M, Zucchini E, Delfino E, Gueli C, Mondragon N, Carli S, Fadiga L and Stieglitz T 2018 Glassy carbon electrocorticography electrodes on ultra-thin and finger-like polyimide substrate: performance evaluation based on different electrode diameters *Materials* **11** 2486
- [54] Vomero M et al., 2018 Achieving ultra-conformability with polyimide-based ECoG arrays *Proc. Annual Int. Conf. IEEE Engineering in Medicine and Biology Society, EMBS* vol 2018
- [55] Renz A F, Lee J, Tybrandt K, Brzezinski M, Lorenzo D A, Cerra Cheraka M, Lee J, Helmchen F, Vörös J and Lewis C M 2020 Opto-E-dura: a soft, stretchable ecog array for multimodal, multiscale neuroscience *Adv. Healthcare Mater.* **9** 2000814
- [56] Liang Y, Offenhäusser A, Ingebrandt S and Mayer D 2021 PEDOT:PSS-based bioelectronic devices for recording and modulation of electrophysiological and biochemical cell signals *Adv. Healthcare Mater.* **10** 2100061
- [57] Lim S, Park H, Yamamoto G, Lee C and Suk J W 2021 Measurements of the electrical conductivity of monolayer graphene flakes using conductive atomic force microscopy *Nanomaterials* **11** 2575
- [58] Cui W, Lu W, Zhang Y, Lin G, Wei T and Jiang L 2010 Gold nanoparticle ink suitable for electric-conductive pattern fabrication using in-inkjet printing technology *Colloids Surf. A* **358** 35–41
- [59] Bian P, Wang Y and McCarthy T J 2021 Rediscovering silicones: the anomalous water permeability of 'hydrophobic' pdms suggests nanostructure and applications in water

- purification and anti-icing *Macromol. Rapid Commun.* **42** 2000682
- [60] Valtakari D, Liu J, Kumar V, Xu C, Toivakka M and Saarinen J J 2015 Conductivity of PEDOT:PSS on spin-coated and drop cast nanofibrillar cellulose thin films *Nanoscale Res. Lett.* **10** 1–10
- [61] Stanford M G, Zhang C, Fowlkes J D, Hoffman A, Ivanov I N, Rack P D and Tour J M 2020 High-resolution laser-induced graphene. Flexible electronics beyond the visible limit *ACS Appl. Mater. Interfaces* **12** 10902–7
- [62] Liu Y, Dong X and Chen P 2012 Biological and chemical sensors based on graphene materials *Chem. Soc. Rev.* **41** 2283–307
- [63] Celik N, Manivannan N, Strudwick A and Balachandran W 2016 Graphene-enabled electrodes for electrocardiogram monitoring *Nanomaterials* **6** 156
- [64] Ozturk O and Yapici M K 2019 Muscular activity monitoring and surface electromyography (sEMG) with graphene textiles *Proc. IEEE Sens.* **2019** 1–4
- [65] Grijalvo S and Díaz D D 2021 Graphene-based hybrid materials as promising scaffolds for peripheral nerve regeneration *Neurochem. Int.* **147** 105005
- [66] Zhu H, Liu A, Shan F, Yang W, Barrow C and Liu J 2017 Direct transfer of graphene and application in low-voltage hybrid transistors *RSC Adv.* **7** 2172–9
- [67] Lambert B J and Tang F W 2000 Rationale for practical medical device accelerated aging programs in AAMI TIR 17 *Radiat. Phys. Chem.* **57** 349–53
- [68] Rynes M L, Ghanbari L, Schulman D S, Linn S, Laroque M, Dominguez J, Navabi Z S, Sherman P and Kodandaramaiah S B 2020 Assembly and operation of an open-source, computer numerical controlled (CNC) robot for performing cranial microsurgical procedures *Nat. Protocols* **15** 1992–2023
- [69] Bernhard S M, Lee J, Zhu M, Hsu A, Erskine A, Hires S A and Barth A L 2020 An automated homecage system for multiwhisker detection and discrimination learning in mice *PLoS One* **15** e0232916